Coarse-Grained Simulations of the HIV-1 Matrix Protein Anchoring: Revisiting Its Assembly on Membrane Domains

Landry Charlier,[†] Maxime Louet,[†] Laurent Chaloin,[‡] Patrick Fuchs,[§] Jean Martinez,[†] Delphine Muriaux,[‡] Cyril Favard,[‡*] and Nicolas Floquet[†*]

[†]Institut des Biomolécules Max Mousseron (IBMM), CNRS UMR5247, Université Montpellier 1, Université Montpellier 2, Faculté de Pharmacie, Montpellier cedex 05, France; [‡]Centre d'études d'agents Pathogènes et Biotechnologies pour la Santé (CPBS) CNRS-UMR 5236, Université Montpellier 1 – Université Montpellier 2, Montpellier Cedex 5, France; and [§]Dynamique des Structures et Interactions des Macromolécules Biologiques INTS, INSERM UMR-S665, Université Paris Diderot, Alexandre Cabanel, Paris

ABSTRACT In the accepted model for human immunodeficiency virus preassembly in infected host cells, the anchoring to the intracellular leaflet of the membrane of the matrix domain (MA) that lies at the N-terminus of the viral Gag protein precursor appears to be one of the crucial steps for particle assembly. In this study, we simulated the membrane anchoring of human immunodeficiency virus-1 myristoylated MA protein using a coarse-grained representation of both the protein and the membrane. Our calculations first suggest that the myristoyl group could spontaneously release from its initial hydrophobic pocket before MA protein interacts with the lipid membrane. All-atom simulations confirmed this possibility with a related energy cost estimated to be ~5 kcal.mol^{-1}. The phosphatidylinositol (4,5) bisphosphate (PI(4,5)P_2) head binds preferentially to the MA highly basic region as described in available NMR data, but interestingly without flipping of its 2′ acyl chain into the MA protein. Moreover, MA was able to confine PI(4,5)P_2 lipids all around its molecular surface after having found a stable orientation at the membrane surface. Our results suggest that this orientation is dependent on Myr anchoring and that this confinement induces a lateral segregation of PI(4,5)P_2 in domains. This is consistent with a PI(4,5)P_2 enrichment of the virus envelope as compared to the host cell membrane.

INTRODUCTION

The human immunodeficiency virus (HIV) genome encodes for a precursor Gag polyprotein that contains all the elements required for the assembly of new virus particles (1). The matrix protein (MA protein), located at the N-terminus of this precursor, is responsible for its anchoring to the host cell plasma membrane via a *N*-myristoylated glycine residue and a highly basic region (HBR) that includes the three Arg-22, Lys-27, and Arg-76 residues (2,3). The presence of the myristate (Myr) considerably increases the affinity of MA for membranes and is absolutely required for virus replication (4,5), even if electrostatic interactions are the main features for protein-membrane interactions (6,7). Furthermore, the preferential binding of MA to negatively charged membranes is enhanced by the interactions between the phosphatidylinositol (4,5) bisphosphate (PI(4,5)P_2) of the membrane and the HBR motif of MA. Mutations of the latter are also known to deeply alter the membrane binding and change cellular Gag localization (8,9). Finally, lipidomic studies have shown that the lipid membrane compositions of both the host cell plasma membrane and the virus could be significantly different, the latter being particularly enriched in the anionic lipid PI(4,5)P_2 (10). Altogether, these results point out the intricate role of the Myr, HBR of MA, and PI(4,5)P_2 in the first steps of virus assembly. The structure of the Myr-MA protein was previously solved by NMR, showing that the Myr group is preferentially sequestrated in a highly hydrophobic pocket inside the protein (Protein Data Bank (PDB): 2H3I) (11). Other NMR data from the same group confirmed the ability of MA to bind PI(4,5)P_2 in the HBR, located on the other side of the Myr in the protein (PDB: 2H3V). From these two structures, the hypothesis of a myristoyl switch was born, in which binding of PI(4,5)P_2 to the HBR motif might promote Myr exposure by, or along with, sequestration of the 2′ unsaturated acyl chain of the PI(4,5)P_2 in another hydrophobic pocket, suggesting therefore that the complex Gag:PI(4,5)P_2 might segregate into rafts or liquid-ordered lipid domains (11). Among other residues, the role of Trp-36 was particularly important in this interaction, because it was implicated in the penetration of the 2′ unsaturated acyl chain of the lipid into the protein (11). This model however suffers from several weak points. First, recent experimental evidences argue for a binding of Gag to the liquid-disordered phase of model membranes (12). Second, it has been shown that the equilibrium between sequestrated and exposed Myr required only minor conformational changes of the protein and was sensitive to both pH and/or Gag oligomerization (13,14). It was also suggested that the exposed Myr might only exist in the trimeric form of the protein, which was also solved by x-ray crystallography (15), whereas it was much more buried in the monomer (14). However, the lack of any significant conformational rearrangements between

Submitted April 11, 2013, and accepted for publication December 6, 2013.

*Correspondence: nicolas.floquet@univ-montp1.fr or cyril.favard@cpbs.cnrs.fr

Patrick Fuchs' present address is Dynamique des membranes et trafic intracellulaire, Institut Jacques Monod, CNRS UMR7592, Université Paris Diderot, Sorbonne Paris Cité, 75205 Paris, France.

Editor: Scott Feller.

0006-3495/14/02/0577/9 $2.00

http://dx.doi.org/10.1016/j.bpj.2013.12.019

the isolated and the interacting monomers does not explain such differences at the molecular scale. Finally, and in contradiction, more recent data have suggested that the Myr could also be exposed in the monomer after encapsulation into reverse micelles (16). Therefore, the exact mechanism by which Myr-MA anchors to lipid membranes containing $PI(4,5)P_2$ is still a matter of debate. To decipher this putative mechanism, we have used coarse-grained (CG) and all-atom molecular dynamics (MD) simulations. In this study, we show that the Myr can be released from its hydrophobic pocket before Myr-MA reaches the surface of the lipid membrane. We also show that the $PI(4,5)P_2$ polar head interacts with the HBR as described by NMR but that the 2′ acyl chain of this lipid stays within the lipid membrane. Finally, we show that binding of Myr-MA to membrane induces a lateral enrichment of $PI(4,5)P_2$ around the protein.

MATERIALS AND METHODS

The HIV-1 MA protein coordinates have been built from the first frame of the PDB entry 2H3I (11). The C-terminal residues of the protein after the Lys-114 in the protein's sequence were not included because of their high flexibility observed in all available NMR structures (root mean-square fluctuations) $>$ 10 Å, see Fig. S1 in the Supporting Material).

CG model

The HIV-1 MA protein was mapped into a CG representation with the MARTINI force field (17,18). An elastic network with a constant force of 500 $kJ.mol^{-1}.nm^{-2}$ was included between residues distant less than 0.9 nm, excluding the first nine N-ter residues (Gly-2 to Gly-10). CG spheres for the aliphatic moiety of the Myr group were derived from already existing parameters in the force field including CG spheres available for the 1,2-dimyristoyl-*sn*-glycero-3-phosphocholine lipid. The CG parameters for the N-terminal Myristoylated Glycine (named GLM) can be found in the Supporting Material. The membrane has been built from an equilibrated model of a bilayer containing 128 1-palmitoyl-2-oleoyl-*sn*-phosphocholine (POPC) molecules as available on the website (http://www.softsimu.net/downloads.shtml) that was automatically mapped to a CG model with self-developed tools. The membrane was then replicated in the *X* and *Y* directions leading to 512 POPC molecules, before progressively modified to obtain a symmetric bilayer of 55% POPC, 5% PIP2, 15% 1-stearoyl-2-oleoyl-*sn*-glycero-3-phospho-L-serine (SOPS), and 25% 1-palmitoyl-2-oleoyl-*sn*-glycero-3-phosphoethanolamine (POPE). Water molecules and counter-ions (203 Na^+) were added to neutralize the global charge, so that the final system was further minimized and equilibrated during a first simulation of 1.5 μs. Using the last snapshot of this simulation, the *Z* dimension of the box containing all lipid atoms was adjusted so that the CG HIV-matrix model could be inserted at a distance of 3.5 nm. The final dimensions of the simulation box were 12.79 nm $\times$ 12.63 nm $\times$ 18.83 nm along *x*, *y*, and *z* directions, respectively. All the following energy-minimizations and MD simulations have been performed with the Gromacs v4.5.5 software (19). The steepest descent algorithm has been used for the energy minimizations. The MD simulations have been coupled to a Berendsen temperature bath at 300 K with $\tau_T = 1$ ps and a Berendsen pressure bath at 1 bar with $\tau_P = 5$ ps with a time step of 15 fs. The defaults parameters for MARTINI MD simulations have been used, the switching function being applied from 0 to 1.2 nm for Coulomb interactions and from 0.9 to 1.2 nm for Lennard-Jones interactions. For the same system, five independent MD simulations (named Myr(e)1 to Myr(e)5) have been performed by changing the initial velocities and without any constraint applied, for a final time of 6 μs each. Two additional simulations were performed using the same protocol with the polarizable MARTINI force field (20). To test the influence of Myr release, two other simulations (named Myr(s)1 and Myr(s)2) were performed with MARTINI in which harmonic constraints between the SC4 atom of GLM and the backbone atoms of Ala-36, Ile-81, and Leu-84 were added to the elastic network with the same force constant of 500 $kJ.mol^{-1}.nm^{-2}$. To decipher the PIP2 residence time in the HBR region, the Myr(e)1 simulation was continued until reaching 24 μs. Analysis of lipids densities were performed only on the last 1 μs of each simulation and only on the PO4 atoms using tools available in Gromacs. Tilt angles to the membrane normal were computed as previously described (21), and for each of the four α-helices of the MA protein, using residues ranges G11:K18 (H1), K32:F44 (H2), S54:S67 (H3), and E74:Q90 (H4).

All-atom model

The HIV-1 matrix protein was also simulated with an all-atom representation using the CHARMM27 force field (22) together with the Gromacs v4.5.5 code for MD simulations (19). All-atom simulations were always performed in the absence of membrane. Parameters for the N-ter Myristoylated Gly were automatically designed with the Paramchem Tool (https://www.paramchem.org/) together with the CGENFF force field (23). The system was solvated with TIP3P water molecules, neutralized, and minimized with the steepest descent algorithm before being equilibrated in the NVT ensemble during 100 ps. After this equilibration step, five different unconstrained MD simulations of 600 ns had been performed in the NPT ensemble. The MD simulations were coupled to a V-rescale temperature bath at 300 K with $\tau_T = 0.1$ ps and a Parrinello-Rahman pressure bath at 1 bar with $\tau_P = 2$ ps. The LINCS algorithm was applied so that a time step of 2 fs could be employed. A cutoff of 1 nm was used for the calculation of the nonbonded interactions, with the particle-mesh-Ewald algorithm, for the treatment of long-range electrostatics. Potential of mean force (PMF) calculations related to GLM release were computed by using an umbrella sampling approach, further analyzed with the weighted histogram analysis method (WHAM) procedure (24). The distance between the N atom of the Ile-82 residue and the C21 atom of GLM was chosen as the reaction coordinate subjected to a 1000 $kJ.mol^{-1}.nm^{-2}$ force constant. The release phenomenon was simulated by 40 intermediate windows, in which this distance was increased by steps of 0.05 nm. For each window, a period of 200 ps was used for equilibration before a production phase of 10 ns was obtained, leading to $40 \times 10 = 400$ ns of simulation for each PMF. Only the successive production phases were used for the final reconstruction of the PMFs. Release experiments were conducted on four different starting points (0 ns, 100 ns, 200 ns, 300 ns) that were extracted from one of the unconstrained all-atom MD simulations of the same system. Two different simulations were performed on each of these four different points leading to eight fully independent PMFs. Only the mean value and standard deviations computed from these simulations were reported (see Fig. 2) for more clarity. Analyses of the data were performed by combining both self-developed scripts and available tools in Gromacs (19) and VMD (25).

All the CG/all-atom simulations performed in this study have been summarized in a table that was provided in the Supporting Material.

RESULTS

Anchoring to the membrane of the Myr-MA protein

Electrostatic interactions drive the first step of Myr-MA binding to the membrane

Starting from its NMR structure (11), we mapped the Myr-MA protein to a CG representation using the MARTINI force field (17,18). An elastic network model was then

applied to the protein to prevent any undesired large conformational rearrangements that can occur with such models on the μs timescale. The N-ter residues 2–10, were not included in this elastic network to permit both the release of Myr and loop motions consistent with NMR data (11). For the MA protein, the use of an elastic network was particularly justified because a very low degree of flexibility was observed among all existing structures in the PDB. To confirm that, root mean-square fluctuations of the protein backbone atoms were computed along the obtained CG simulations and directly compared to those deduced from both NMR data (PDB structures 1UPH, 2H3F, 2H31, 2H3Q, 2H3V, 2H3Z, 2JMG, and 2NV3) and all-atom simulations performed with the CHARMM force field ; the obtained graphs reported in Fig. S1 confirmed that the use of the elastic network did not affect the overall flexibility of the protein and successfully reproduced the experimental fluctuations described by available structures. Using this model, we simulated the putative mechanism of anchoring of the Myr-MA protein to a membrane model, which composition was adapted from the cell plasma membrane inner leaflet (10) (55% POPC, 25% POPE, 15% SOPS, and 5% SAPI(4,5)P_2 (see the Supporting Material for explanation)). Parameters for PI(4,5)P_2 were inspired from other preexisting lipids in the same force field and from previously published studies (26,27) (detailed parameters for PI(4,5)P_2 were supplied in the Supporting Material). In each of the five obtained trajectories (noted Myr(e)1 to Myr(e)5), the anchoring of the protein to the membrane occurred on the μs timescale (see Fig. 1 *A* and Movie S1). After this step, analyses of the resulting tilt angles with respect to the membrane normal for each of the four α-helices of Myr-MA (reported respectively in *blue*, *red*, *yellow*, and *green* in both Fig. 1 *B* and Fig. 1 *C*) clearly showed that the protein found a stable and perfectly reproducible orientation at the membrane surface in each of the five simulations. Of importance, this orientation was consistent not only with the existing NMR data (11), but also with the previously published data from neutron reflectivity (6). Additionally, because the C-terminal end of the MA protein was also facing the solvent in this orientation, this model was also compatible with the presence of the whole HIV-1 Gag precursor at the membrane surface. As compared to the Myr(e) protein, the orientation of the Myr(s) protein (Myr(s)1, Myr(s)2 simulations) in which the Myr group was forced to stay in its initial position, was slightly different, corresponding to a rotation of ~20°of the protein around the helix 2 axis, and finally resulting in a nearly parallel orientation of the helix 1 with respect to the membrane surface (see Fig. 1 *B* and Fig. 1 *C*).

The MARTINI force field is particularly well suited for the assessment of membrane segment orientation and partitioning (28,29). Interestingly, inclusion of the Myr group in the elastic network did not prevent MA:membrane association, thus confirming that MA:membrane interactions were mainly electrostatically driven (30). In agreement, depleting

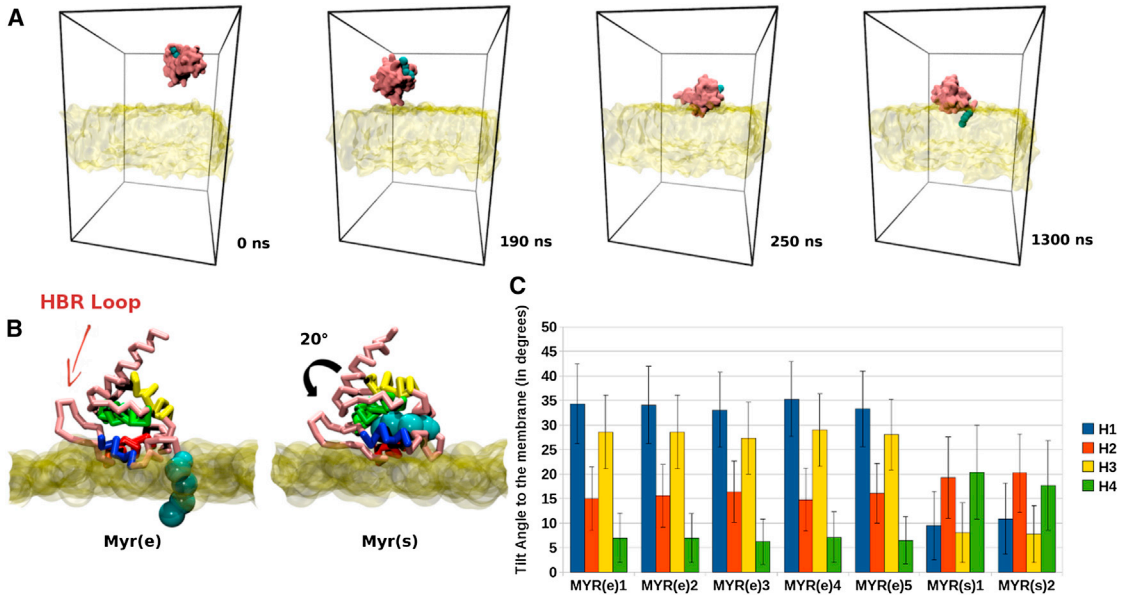

FIGURE 1 (*A*) Representative snapshots from an anchoring experiment of the Myr-MA protein to our membrane model; Myr residue at the N-terminus of HIV-1 MA was reported in blue spheres, whereas the membrane was reported in yellow surface. Water molecules were removed from the figure for more clarity. (*B*) When Myr release was prevented (Myr(s), *on the right*), the protein found a stable orientation at the membrane surface corresponding to a 20°rotation of that found for the Myr(e) MA (*on the left*) HBR in which PI(4,5)P_2 binds. Helices 1, 2, 3, and 4 of the protein were colored in blue, red, yellow, and green, respectively. (*C*) Stabilized values of the tilts to the membrane found for each of the four α-helices of the protein after membrane anchoring with both Myr exposed (Myr(e)) and Myr sequestrated (Myr(s)) models. Color coding for the helices was the same as in (*B*). To see this figure in color, go online.

the membrane of its anionic PS and PI(4,5)P_2 lipids interestingly contributed to the disruption of the Myr(s) protein:membrane interactions over time, the protein no longer staying at the membrane surface (data not shown). At this step, because the electrostatic interactions seemed to play an important role, simulations of the Myr(e) system were also performed with the polarizable MARTINI force field (20). Nevertheless, no anchoring of the MA protein was observed during the two obtained 6 μs simulations whereas, in the five nonpolarizable MARTINI simulations, the anchoring always occurred at the latest after 1.5 μs. The possible reasons for this absence of anchoring on μs timescale simulations using the polarizable MARTINI force field are discussed in the Supporting Material.

Myr release occurs before membrane anchoring of Myr-MA

In each of the five obtained trajectories (noted Myr(e)1 to Myr(e)5), the Myr group was spontaneously releasing out of its binding pocket on the 100 ns timescale and contributed, in each case, to the anchoring of the protein to the membrane on the μs timescale (see Fig. 1 *A* and Movie S1). We considered that the Myr group was released when all the CG spheres representing its hydrophobic chain were outside its initial pocket. After release, we observed that the Myr group remained most of the time at the protein surface to prevent too many unwished contacts with surrounding water molecules. Myr release is thought to occur after MA binding to PI(4,5)P_2 in the Myristoyl switch model, whereas it constituted the first observed step in our CG simulations. Therefore, Myr release out of the MA hydrophobic pocket and the equilibrium between its sequestrated and exposed conformations are key questions. In CG simulations, molecular diffusion is accelerated because of reduced friction (17) and could be the reason for this release. It was therefore important to verify this behavior using all-atom MD simulations performed with the CHARMM force field (22). Starting with the same NMR structure as the one used for CG MD simulations, five different all-atom unconstrained MD simulations of 600 ns were first obtained for the protein in a box of water. As already mentioned before, Fig. S1 confirmed that the chosen force field allowed successful modeling of the flexibility of the protein, in good agreement with both CG and experimental profiles of flexibility. Of importance, the Myr group was spontaneously releasing from its pocket in one of these simulations, after 170 ns, thus confirming that this release could occur at ambient temperature, even using an all-atom representation of both the protein and the solvent.

To completely validate this mechanism, it was also important to assess the putative energy cost for spontaneous Myr release out of its hydrophobic pocket in the absence of PI(4,5)P_2. For this purpose, PMFs were further reconstructed from extensive MD simulations using an umbrella sampling protocol together with the weighted histogram analysis method algorithm (24). The distance between the N atom of the Ile-82 and the C21 atom of Myr was chosen as the reaction coordinate (Fig. 2). A shoulder was observed in the resulting PMFs at a distance of ~1.7 nm that was corresponding to an energy cost of ~5 kcal.mol^{-1} (see Fig. 2). At this step, the Myr group was already completely out from its initial binding pocket but still in contact with the protein surface, in a position closely related to that previously observed in CG simulations. Such an energy cost of 5 kcal.mol^{-1} corresponds to a dissociation constant of ~200 μM, and suggests a significant equilibrium between sequestrated and exposed Myr in water, even for the monomer. Fig. 2 further showed that an additional cost of 3 kcal.mol^{-1} was required to obtain a full exposure to the solvent of the Myr group, at a distance of 2.5 nm.

Myr-MA:membrane interactions

Insertion of Myr

In the CG simulations, and after contact with the membrane, the Myr group was completely buried into the phospholipid bilayer, as already mentioned in previously published experimental studies (31), keeping a mostly extended conformation, as also described (31,32) (see Fig. S2). Interestingly, and in addition to modifying the protein orientation (see Fig. 1 *B* and Fig. 1 *C*), it was observed that the anchoring of the Myr group to the membrane decreased significantly the order parameters of immediately surrounding lipids

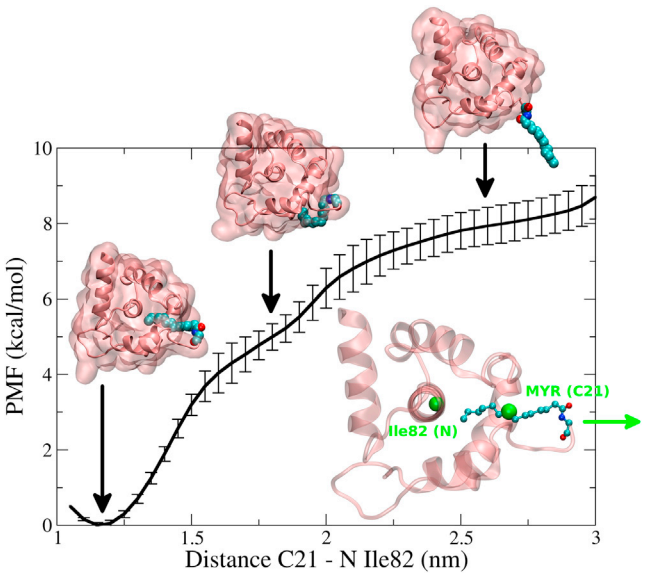

FIGURE 2 Results from the all-atom umbrella sampling simulations of Myr release in the Myr-MA protein using the Ile-82(N):Myr(C21) as a reaction coordinate. Error bars correspond to the standard deviations computed among the eight independent simulations. To see this figure in color, go online. To see this figure in color, go online.

(Fig. S3, *dashed lines*). Order parameters computed for all lipids, in the presence or in the absence of the protein confirmed that this effect was much more pronounced around the Myr (Fig. S3). Such a disorder has already been observed by NMR measurements during the interaction of myristoylated Src peptides with charged membranes (33).

The membrane anchored Myr-MA captures PI(4,5)P_2

Using the obtained CG simulations trajectories, we computed the number of lipids present in a sphere of 10 Å around the protein either 1), just after Myr anchoring or 2), just after the protein found a stable orientation at the membrane surface. The resulting numbers of PI(4,5)P_2, PC, PE, and PS were reported in Fig. 3 *A*. These analyzes clearly showed an increased localization of the PI(4,5)P_2 at the protein surface at step 2, with a mean number of PI(4,5)P_2 increasing from 4 to 5. Such a slight increase of only one lipid (representing however an increase of 25%) was perfectly reproducible among the five obtained simulations (see error bars reported in the same figure). In the same time, the numbers of both POPC and POPE were much more stable suggesting no particular specific recruitment of these lipids. On the contrary, a mean decrease of one SOPS molecule was observed. The plots of lipid densities during step 2 in Fig. 3 *B* further showed that the PI(4,5)P_2 was present all around the protein surface but statistically more located at the proximity of the HBR of the protein. PC, PE, and PS lipids were more uniformly distributed. This overdistribution of PI(4,5)P_2 near the HBR of the protein was in perfect agreement with NMR data showing that the binding of this lipid effectively occurs in this region (11). Interestingly, and as shown in Fig. 3 *C*, we observed that the polar head of the PI(4,5)P_2 molecule bound to the HBR exactly adopted the same orientation as that described by available NMR data (PDB: 2H3V (11)), e.g., by establishing polar interactions between each of its three phosphates and surrounding residues Arg-22, Lys-27, and Arg-76, respectively. Using the results of a longer CG simulation of 24 μs, the mean residence time of the PI(4,5)P_2 molecule in the HBR was estimated to ~1 μs. During such a long MD simulation, we observed that each of the 13 PI(4,5)P_2 molecules present on the same leaflet of the membrane was successively visiting this position in the protein (see Fig. S4).

The 2′ acyl chain of the PI(4,5)P_2 stays in the lipid membrane

Contrary to the previously described extended lipid conformation phenomenon, no interaction involving the 2′-fatty acid chain of PI(4,5)P_2 in to MA occurred (11), the fatty acid chain, logically preferring to maintain contacts with other surrounding acyl chains of the lipids present in the

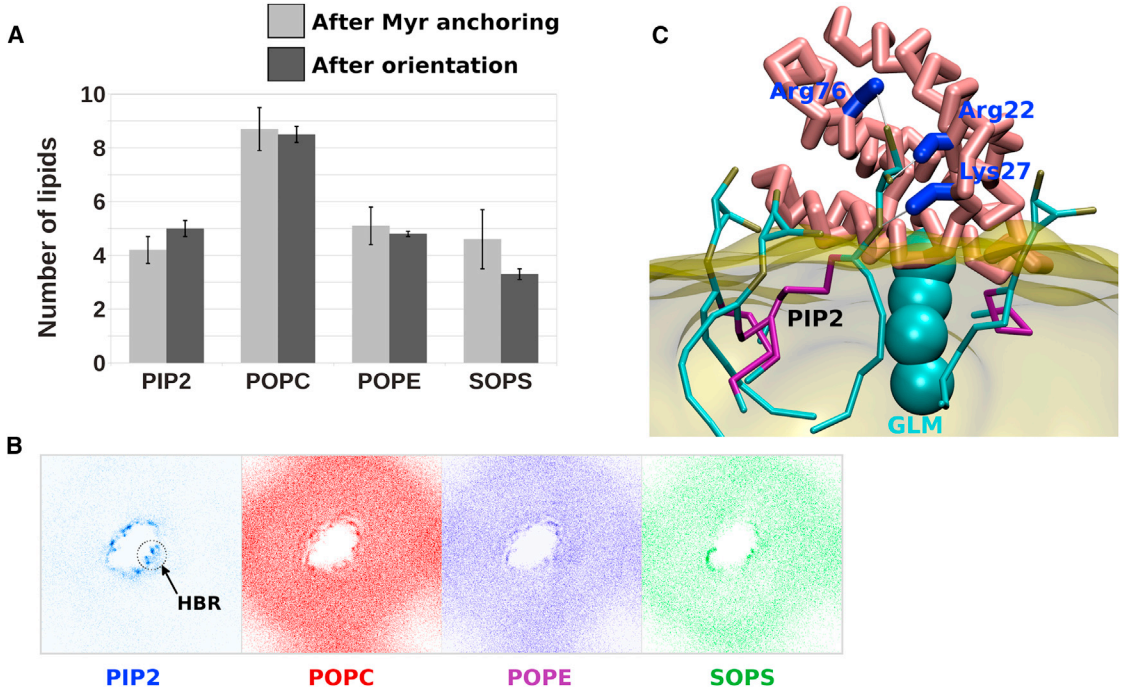

FIGURE 3 (*A*) Count of lipids (PIP2, POPC, POPE, SOPS) numbers around 10 Å of the Myr(e)-MA protein: (*gray*) after Myr anchoring and (*black*) after the protein found a stable orientation at the membrane surface. Error bars correspond to the standard values computed among the five independent anchoring simulations. (*B*) Densities computed for each type of lipids (*Blue*: PI(4,5)P_2, *Red*: PC, *Purple*: PE, *Green*: PS) after the Myr(e)-MA protein found a stable orientation at the membrane surface ; analyses were performed only on the phosphate PO4 particle common to all types of lipids and on the last μs of each trajectory. (*C*) In the region that was the most occupied by PI(4,5)P_2, the lipid head was binding exactly as described by available MA:PI(4,5)P_2 NMR structures. However, the 2′-fatty acid chain of PI(4,5)P_2 was not flipping into the protein in contrast to the extended lipid conformation hypothesis described elsewhere (11). To see this figure in color, go online.

membrane, rather than going outside the bilayer. Actually, the acyl chains of the lipid bound to MA in NMR studies were two- to threefold shorter (di-C4 or di-C8-PI(4,5)P_2) than the one used in our simulations (1-stearoyl-2-arachidonoyl-PI(4,5)P_2), the latter better reflecting the ones naturally present in cell plasma membranes and HIV-1 viruses (10). In agreement, the orientation of residue Trp-36 in our model was completely different from that described by NMR data in water (11). In the NMR model, Trp-36 was suggested to play a direct and key role in the binding of the 2′ acyl chain of PI(4,5)P_2 in the protein, whereas this residue was fully embedded in the bilayer in our simulations (see Fig. S5). From our model, it can therefore be suggested that Trp-36 could contribute, together with other hydrophobic residues including Va-l7, Leu-13, and Val-35, to both membrane binding and protein orientation at the membrane surface.

Binding of PI(4,5)P_2 is lost by specific mutations in the HBR

The electrostatic recruitment of PI(4,5)P_2 by a cellular protein has already been observed with similar methods (27). To confirm the specificity of this binding, three additional anchoring simulations were performed in which the residues constituting the HBR were mutated into alanines (R22A+K27A+R76A). These mutations are known to considerably affect both PI(4,5)P_2 binding and membrane avidity (7). Interestingly, the resulting graph reported in Fig.4 *A* showed that the introduced mutations led to no increase of PI(4,5)P_2 around the protein, although the latter found the same orientation at the membrane surface as the wild-type protein. A comparison between Fig. 4 *B* and Fig. 3 *B* confirmed that the lack of PI(4,5)P_2 was mostly located around the mutated HBR. Not surprisingly, it appeared that the missing PI(4,5)P_2 molecules in this region could be replaced by PS molecules (Fig. 4 *B*). The putative binding mode of PS molecule was reported in Fig. 4 *C* showing its interaction with Lys-26, Lys-30, and Lys-32.

Capture of PI(4,5)P_2 is orientation-dependant

We have shown before that Myr(e) and Myr(s)-MA did not adopt the same orientation at the membrane surface, the rotation of 20° of the whole Myr(s)-MA protein contributing to a different position of the HBR loop, face downward on the membrane (see Fig. 1 *B*). Therefore, comparing the lipid numbers around the protein to those computed for Myr(e)-MA seemed meaningless. However, and as performed for the Myr(e)-MA protein, we analyzed lipid densities around the Myr(s)-MA (see Fig. 5 *A*). Interestingly, it was observed that the PI(4,5)P_2 distribution all around the protein was significantly affected by this change of orientation, this lipid being generally less present at the protein surface, and totally absent in the HBR region. As already observed for the Myr(e)-HBR mutant, lacking PI(4,5)P_2 at proximity of the HBR loop were replaced by PS molecules. In this case, it was rather due to the change of orientation of the protein at the membrane surface, permitting residues Lys-27, Arg-22, and Arg-76 to get closer to the polar heads of PS molecules (see Fig. 5 *B*).

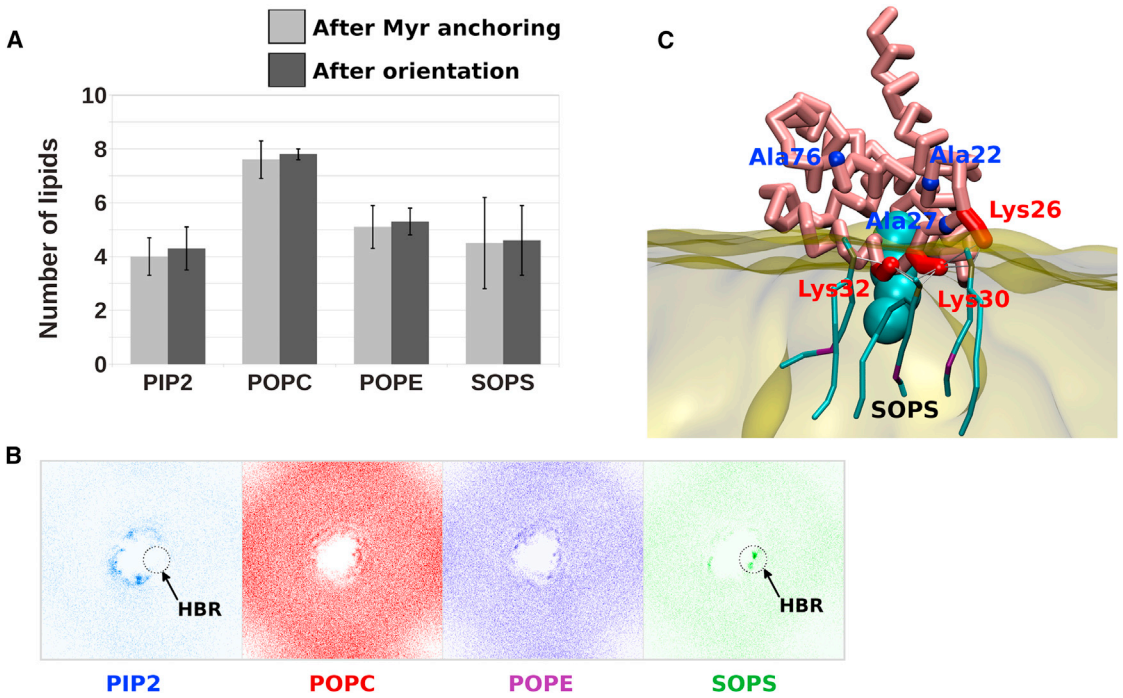

FIGURE 4 The same analyses as those described in Fig.3 were performed on the HBR mutated protein showing a depletion of PI(4,5)P_2 in the corresponding region, supplemented by the binding of PS, as described in (*C*). To see this figure in color, go online.

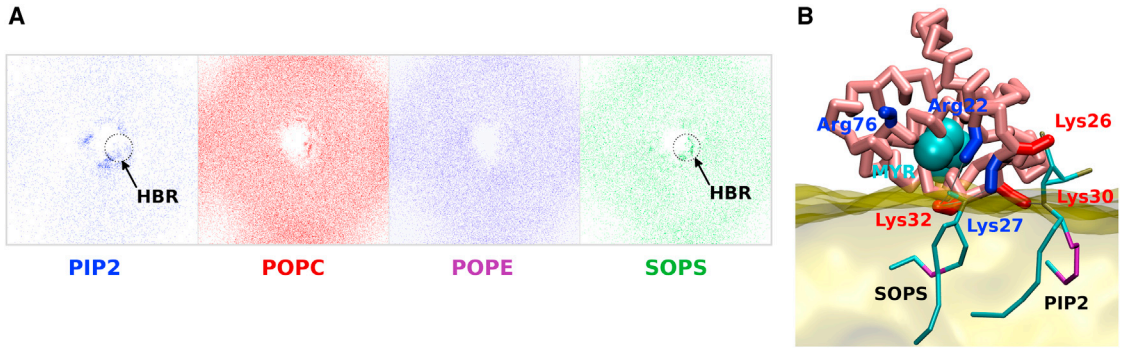

FIGURE 5 (*A*) Densities computed for each type of lipids (*Blue*: PI(4,5)P_2, *Red*: PC, *Purple*: PE, *Green*: PS) after the Myr(s)-MA protein was at the membrane surface. Analyses were performed only on the phosphate PO4 particle common to all types of lipids and on the last μs of each trajectory. (*B*) PS binding mode observed for the Myr(s)-MA protein. To see this figure in color, go online.

DISCUSSION

In this study, we have investigated the putative mechanism of Myr-MA anchoring to a membrane containing PI(4,5)P_2. Our results suggest that the beginning of this anchoring is mainly electrostatically driven as it has already been suggested for other acylated proteins containing basic motifs (34–36) and also from neutron reflectivity studies (6). During these first steps, before reaching the vicinity of the lipid membrane, a release of the Myr from its hydrophobic pocket occurred. Employing free energy calculations, the cost required for Myr release out from its hydrophobic pocket was only ~5 kcal.mol^{-1}, suggesting a significant equilibrium between sequestrated and exposed Myr in water, even for the monomer. Interestingly, this energy cost is lower than the gain expected for the subsequent Myr insertion into the membrane, in the range -5.2: -10.6 kcal.mol^{-1} (37), suggesting that a mechanism with two successive release + insertion steps would be energetically favorable. This is in agreement with recent data obtained by NMR with bicelles and micelles, suggesting that the Myr residue is more readily exposed in the proximity of a lipid bilayer (16,38). Using related modeling methods, it would therefore have been interesting to also quantitatively evaluate the energy required for Myr reintrance into the same pocket, when MA is far from the lipid bilayer. However, such an evaluation is thought to be much harder (if not impossible). Indeed, we observed that, after Myr release, the mobility of the N-terminal loop of the protein that shares the Myr group was much increased. This might prevent a proper sampling of all the possible binding pathways. Moreover, using the Fpocket software (39,40), plotting the hydrophobic pocket's volume along the obtained releasing trajectories clearly showed a significant collapse of this pocket after Myr release, this volume decreasing almost by a half (see Fig. S6). Such a collapse could also contribute to the increase of the required energy for Myr reintrance into the pocket, perhaps explaining why such a reentry has not been observed during our CG or all-atom simulations.

Our results interestingly show that the insertion of the Myr into the phospholipid bilayer is strictly required for the protein to find a correct orientation at the membrane surface. Indeed, the insertion of the Myr causes the helix 1 to swing, allowing a more favorable positioning of the HBR for specific interaction with PI(4,5)P_2. Therefore, after Myr exposure and having found this proper orientation at the membrane surface, the HIV-1 Myr-MA protein was able to confine PI(4,5)P_2 lipids all around its surface, and more specifically in the HBR, but without any flipping of its acyl chains (2′ or 1′). Specificity of PI(4,5)P_2 binding to the HBR can be directly correlated to the quite long residence time of the lipid, ~1 μs (computed from our MD simulations) and indirectly to the lack of interaction when mutations were introduced in the corresponding binding region. Nonspecific accumulation of PI(4,5)P_2 around the Myr-MA protein was mainly due to electrostatics (see Fig. S7) and could nicely contribute to Gag multimerization as a cooperative effector. This could lead to, as it has already been seen for other proteins (27,41), MA-induced PI(4,5)P_2 partitioning into domains during HIV-1 assembly as previously proposed (42) and finally ending in PI(4,5)P_2 enrichment of the virus envelope as compared to the host cell plasma membrane (10,43). Our results clearly show that the time sequence of MA interaction with lipid membranes could be simplified into three main steps: i), long-range, nonspecific electrostatic interactions to reach the membrane surface, Myr exposure occurs during this step; ii), anchoring of the Myr leading to a correct orientation of the MA protein; and iii), PI(4,5)P_2 headgroup-specific interaction with the HBR motif of the protein without any flipping of the lipid acyl chains, contributing on longer timescales to a lateral segregation of PI(4,5)P_2 all around the protein, within the plane of the lipid membrane.

Future work includes the remapping of the obtained CG models into an all-atom representation to perform long MD simulations of the membrane-anchored Myr-MA protein. Using the resulting conformational sampling of the PI(4,5)P_2: Protein complex, computer-assisted drug design

will be employed to try to identify/design ligands able to bind to the HBR motif of Myr-MA and prevent or inhibit Myr-MA:membrane association and/or orientation.

SUPPORTING MATERIAL

Seven figures, one table, one movie, supporting data, and reference (44) are available at http://www.biophysj.org/biophysj/supplemental/S0006-3495(13)05811-6.

We thank University Montpellier 1 for financial PhD/post-doctoral support of L.C. and M.L..

This work was realized with the support of HPC@LR, a Center of competence in High-Performance Computing from the Languedoc-Roussillon region, funded by the Languedoc-Roussillon region, the Europe and the Université Montpellier 2 Sciences et Techniques. The HPC@LR Center is equipped with an IBM hybrid Supercomputer.

REFERENCES

1. Adamson, C. S., and E. O. Freed. 2007. Human immunodeficiency virus type 1 assembly, release, and maturation. *Adv. Pharmacol.* 55:347–387.
2. Zhou, W., L. J. Parent, …, M. D. Resh. 1994. Identification of a membrane-binding domain within the amino-terminal region of human immunodeficiency virus type 1 Gag protein which interacts with acidic phospholipids. *J. Virol.* 68:2556–2569.
3. Hamard-Peron, E., and D. Muriaux. 2011. Retroviral matrix and lipids, the intimate interaction. *Retrovirology.* 8:15.
4. Göttlinger, H. G., J. G. Sodroski, and W. A. Haseltine. 1989. Role of capsid precursor processing and myristoylation in morphogenesis and infectivity of human immunodeficiency virus type 1. *Proc. Natl. Acad. Sci. USA.* 86:5781–5785.
5. Bryant, M., and L. Ratner. 1990. Myristoylation-dependent replication and assembly of human immunodeficiency virus 1. *Proc. Natl. Acad. Sci. USA.* 87:523–527.
6. Nanda, H., S. A. K. Datta, …, J. E. Curtis. 2010. Electrostatic interactions and binding orientation of HIV-1 matrix studied by neutron reflectivity. *Biophys. J.* 99:2516–2524.
7. Murray, P. S., Z. Li, …, D. Murray. 2005. Retroviral matrix domains share electrostatic homology: models for membrane binding function throughout the viral life cycle. *Structure.* 13:1521–1531.
8. Chukkapalli, V., S. J. Oh, and A. Ono. 2010. Opposing mechanisms involving RNA and lipids regulate HIV-1 Gag membrane binding through the highly basic region of the matrix domain. *Proc. Natl. Acad. Sci. USA.* 107:1600–1605.
9. Ono, A., S. D. Ablan, …, E. O. Freed. 2004. Phosphatidylinositol (4,5) bisphosphate regulates HIV-1 Gag targeting to the plasma membrane. *Proc. Natl. Acad. Sci. USA.* 101:14889–14894.
10. Chan, R., P. D. Uchil, …, M. R. Wenk. 2008. Retroviruses human immunodeficiency virus and murine leukemia virus are enriched in phosphoinositides. *J. Virol.* 82:11228–11238.
11. Saad, J. S., J. Miller, …, M. F. Summers. 2006. Structural basis for targeting HIV-1 Gag proteins to the plasma membrane for virus assembly. *Proc. Natl. Acad. Sci. USA.* 103:11364–11369.
12. Keller, H., H.-G. Kräusslich, and P. Schwille. 2012. Multimerizable HIV Gag derivative binds to the liquid-disordered phase in model membranes. *Cell. Microbiol.* 15:237–247.
13. Fledderman, E. L., K. Fujii, …, J. S. Saad. 2010. Myristate exposure in the human immunodeficiency virus type 1 matrix protein is modulated by pH. *Biochemistry(Mosc.).* 49:9551–9562.
14. Tang, C., E. Loeliger, …, M. F. Summers. 2004. Entropic switch regulates myristate exposure in the HIV-1 matrix protein. *Proc. Natl. Acad. Sci. USA.* 101:517–522.
15. Hill, C. P., D. Worthylake, …, W. I. Sundquist. 1996. Crystal structures of the trimeric human immunodeficiency virus type 1 matrix protein: implications for membrane association and assembly. *Proc. Natl. Acad. Sci. USA.* 93:3099–3104.
16. Valentine, K. G., R. W. Peterson, …, A. J. Wand. 2010. Reverse micelle encapsulation of membrane-anchored proteins for solution NMR studies. *Structure.* 18:9–16.
17. Marrink, S. J., A. H. de Vries, and A. E. Mark. 2004. Coarse grained model for semiquantitative lipid simulations. *J. Phys. Chem. B.* 108:750–760.
18. Marrink, S. J., H. J. Risselada, …, A. H. de Vries. 2007. The MARTINI force field: coarse grained model for biomolecular simulations. *J. Phys. Chem. B.* 111:7812–7824.
19. Hess, B., C. Kutzner, …, E. Lindahl. 2008. GROMACS 4: algorithms for highly efficient, load-balanced, and scalable molecular Simulation. *J. Chem. Theory Comput.* 4:435–447.
20. Yesylevskyy, S. O., L. V. Schäfer, …, S. J. Marrink. 2010. Polarizable water model for the coarse-grained MARTINI force field. *PLOS Comput. Biol.* 6:e1000810.
21. Ozdirekcan, S., C. Etchebest, …, P. F. J. Fuchs. 2007. On the orientation of a designed transmembrane peptide: toward the right tilt angle? *J. Am. Chem. Soc.* 129:15174–15181.
22. Brooks, B. R., C. L. Brooks, 3rd, …, M. Karplus. 2009. CHARMM: the biomolecular simulation program. *J. Comput. Chem.* 30:1545–1614.
23. Vanommeslaeghe, K., E. Hatcher, …, A. D. Mackerell, Jr. 2010. CHARMM general force field: a force field for drug-like molecules compatible with the CHARMM all-atom additive biological force fields. *J. Comput. Chem.* 31:671–690.
24. Kumar, S., J. M. Rosenberg, …, P. A. Kollman. 1992. The weighted histogram analysis method for free-energy calculations on biomolecules. I. The method. *J. Comput. Chem.* 13:1011–1021.
25. Humphrey, W., A. Dalke, and K. Schulten. 1996. VMD: visual molecular dynamics. *J. Mol. Graph.* 14:33–38, 27–28.
26. Stansfeld, P. J., R. Hopkinson, …, M. S. P. Sansom. 2009. PIP2-binding site in Kir channels: definition by multiscale biomolecular simulations. *Biochemistry (Mosc.).* 48:10926–10933.
27. van den Bogaart, G., K. Meyenberg, …, R. Jahn. 2011. Membrane protein sequestering by ionic protein-lipid interactions. *Nature.* 479:552–555.
28. Balali-Mood, K., P. J. Bond, and M. S. P. Sansom. 2009. Interaction of monotopic membrane enzymes with a lipid bilayer: a coarse-grained MD simulation study. *Biochemistry.* 48:2135–2145.
29. Wee, C. L., K. Balali-Mood, …, M. S. P. Sansom. 2008. The interaction of phospholipase A2 with a phospholipid bilayer: coarse-grained molecular dynamics simulations. *Biophys. J.* 95:1649–1657.
30. Dalton, A. K., D. Ako-Adjei, …, V. M. Vogt. 2007. Electrostatic interactions drive membrane association of the human immunodeficiency virus type 1 Gag MA domain. *J. Virol.* 81:6434–6445.
31. Vogel, A., T. Schröder, …, D. Huster. 2007. Characterization of the myristoyl lipid modification of membrane-bound GCAP-2 by 2H solid-state NMR spectroscopy. *Biochim. Biophys. Acta.* 1768:3171–3181.
32. Witte, K., B. E. S. Olausson, …, A. Vogel. 2013. Structure and dynamics of the two amphipathic arginine-rich peptides RW9 and RL9 in a lipid environment investigated by solid-state NMR and MD simulations. *Biochim. Biophys. Acta.* 1828:824–833.
33. Scheidt, H. A., and D. Huster. 2009. Structure and dynamics of the myristoyl lipid modification of SRC peptides determined by 2H solid-state NMR spectroscopy. *Biophys. J.* 96:3663–3672.
34. Resh, M. D. 1999. Fatty acylation of proteins: new insights into membrane targeting of myristoylated and palmitoylated proteins. *Biochim. Biophys. Acta.* 1451:1–16.

35. Murray, D., L. Hermida-Matsumoto, …, S. McLaughlin. 1998. Electrostatics and the membrane association of Src: theory and experiment. *Biochemistry.* 37:2145–2159.

36. Murray, D., N. Ben-Tal, …, S. McLaughlin. 1997. Electrostatic interaction of myristoylated proteins with membranes: simple physics, complicated biology. *Structure.* 5:985–989.

37. Pool, C. T., and T. E. Thompson. 1998. Chain length and temperature dependence of the reversible association of model acylated proteins with lipid bilayers. *Biochemistry.* 37:10246–10255.

38. Vlach, J., and J. S. Saad. 2013. Trio engagement via plasma membrane phospholipids and the myristoyl moiety governs HIV-1 matrix binding to bilayers. *Proc. Natl. Acad. Sci. USA.* 110:3525–3530.

39. Le Guilloux, V., P. Schmidtke, and P. Tuffery. 2009. Fpocket: an open source platform for ligand pocket detection. *BMC Bioinformatics.* 10:168.

40. Schmidtke, P., A. Bidon-Chanal, …, X. Barril. 2011. MDpocket: open-source cavity detection and characterization on molecular dynamics trajectories. *Bioinformatics.* 27:3276–3285.

41. McLaughlin, S., and D. Murray. 2005. Plasma membrane phosphoinositide organization by protein electrostatics. *Nature.* 438:605–611.

42. Kerviel, A., A. Thomas, …, D. Muriaux. 2013. Virus assembly and plasma membrane domains: which came first? *Virus Res.* 171:332–340.

43. Ding, L., A. Derdowski, …, P. Spearman. 2003. Independent segregation of human immunodeficiency virus type 1 Gag protein complexes and lipid rafts. *J. Virol.* 77:1916–1926.

44. Bucher, D., Y.-H. Hsu, …, J. A. McCammon. 2013. Insertion of the Ca^{2+}-independent phospholipase A2 into a phospholipid bilayer via coarse-grained and atomistic molecular dynamics simulations. *PLoS Comput. Biol.* 9:e1003156.